International Journal of
INTELLIGENT SYSTEMS AND APPLICATIONS IN ENGINEERING
ISSN:2147-6799 www.ijisae.org Original Research Paper

Detection and Classification of the Brain Tumor Brilliant Jumping Algorithm Optimized W-Net Enabled DCNN

Divya Kumari[1]* and B. K. Anoop[2]

Submitted:14/03/2024 **Revised**: 29/04/2024 **Accepted**: 06/05/2024

Abstract: Brain tumors (BT) have remained a deadly disease across the world in recent years. Though there exist several detection mechanisms and models that provide the basic detection and classification of the tumor, they fail to work with certain parameters such as convergence, computational efficiency, and so on. To prevail over the issue of the conventional methods and to propose the detection as well as the classification model for grading the tumors is developed in this research. The Brilliant Jumping Algorithm Optimized W-Net Enabled Deep Convolutional Neural Network (BW-Net+BDN) is employed in the research of detecting and classifying BTs. The research included W-Net as the segmentation model that is optimized with the Brilliant jumping Algorithm (BJA). Furthermore, the included BJA optimization is the hybridization of the characteristics of the rabbit as well as the coyote to improve the effectiveness of the classifier, and the segmentation model as optimization is utilized in both classification and segmentation. The entire research detects the BT through the BW-Net segmentation model and classifies them based on grades such as normal, mild, and severe through the BDN classification model. The effectiveness of the BW-Net+BDN is analyzed with accuracy, Sensitivity, Specificity, and Balanced Error Rate that achieves 93.23%, 93.39%, 93.77%, and 6.58 respectively.

Keywords: *Brain Tumor, Segmentation, W-Net, Brilliant Jumping Algorithm, and VGG-16*

1. Introduction

The brain, which is the central part of the human contains between 50 and 100 trillion neurons, has been referred to as the nervous system's processor because of its important functions and structural dependencies [1] [2] [3]. Since the brain is the core nervous system, it can be impacted by a variety of illnesses, including Alzheimer's and BTs. Tumors are typically caused by an unregulated development of malignant cells in any section of the body[4]. Tumors are classified into distinct categories as per the traits and the competing therapies that are used. Of all the tumor forms, BTs are said to be the most dangerous and meticulous diseases, requiring a medical professional's clear analysis to accurately classify the tumor [5]. Though the hard skull encloses the brain, the growth of malignant tissues in such regions causes terrific issues, which can be both malignant and non-cancerous BTs. Benign or malignant tumors will cause an increase in intracranial pressure. This will be the reason for mortality or severe lasting brain damage. [6]. Therefore, early BT discovery is crucial for the medical field since it reduces mortality by offering high-quality care.

Clinicians treat tumors using a variety of techniques, including radiation therapy, surgery, and chemotherapy, but therapy utilization constantly depends on the characteristics of the tumor, including its size, form, and composition [7] [8]. Clinical technologies such as MRI provide complete data in the form of segment representations of both healthy and tumorous regions [9][10][11]. Checking for tumor abnormalities remains a tough challenge, nevertheless, because of the large number of slices. It consumes high effort and time for clinical specialists to examine each slice individually [12]. Furthermore, a tumor cannot be identified in every slice by the human eye alone [13]. Numerous choices are available in medical clinics to assist patients in identifying health issues. Several novel concepts in the realm of computerized medical assistance systems have been introduced by recent developments in computer science. Hospitals are outfitted with modern equipment, as is evident. Organisms and tissue are observed with new optics. Multimedia platforms are useful for exams. Testing and results of scans are assessed on monitors, which offer a high-quality display useful for in-depth analyses. Radiography, or more specifically, different RTG and CT screening methods, is one of the more recent disciplines where computer science has proven to be quite beneficial [14].

Various machine learning (ML) techniques are developed for classifying BTs that includes numerous imaging modalities such as CT, MRI, and so forth. A model for categorizing various glioma grades using KNN and SVM classifiers was created in [15]. A technique was developed in [16] to categorize the cancerous regions into abnormal or normal by utilizing Principal Component Analysis

[1]*Srinivas University, Chelairu Road Srinivas Nagar, Mukka, Surathkal, Mangaluru, Karnataka, India, 574146*
[2]*Srinivas University, Chelairu Road Srinivas Nagar, Mukka, Surathkal, Mangaluru, Karnataka, India, 574146*
** Corresponding Author Email: divyakumari.ccis@srinivasuniversity.edu.in*

(PCA) to minimize the feature dimensions and applying the Discrete Wavelet Transform (DWT) for feature mining. The features are used in KNN and ANN to accurately categorize the images. A method was developed in [17] to enhance the tumor classification performance by first utilizing picture dilation to see the tumor regions and then splitting the parts to identify the malignancies. Three techniques were used in this instance to extract the features, including Bag of Words (BOW) and Gray Level Co-occurrence Matrix (GLCM), and by enhancing the tumor regions, the accuracy of the results was increased. Furthermore, utilizing SVM and GA, the binary classifiers [18] were applied to various classes to ascertain if the tumor location is benign, malignant, or both. A three-level back-propagation neural network was developed in [19] to use several features in the differentiation of benign and malignant tumors.

The research aims at developing detection and classification model of the BT with greater efficiency. The model utilized the BW-Net to segment the tumor as well as the non-tumor regions, which aid in achieving the severity of the BT in classification. The extraction of the Region of Interest (ROI) is performed initially to observe more interested regions from the image inputs. The feature vector is obtained from the process of feature extraction, which is carried out by several techniques that achieve the maximum efficiency and the minimum error rate. The major contributions of the research are as follows,

- **BHA optimization:** BHA optimization is the integration of the traits of the rabbit and the coyote. The combination of the characters aids the classifier to work with the convergence issue and the time complexity.
- **BW-Net:** The model is utilized to segment the tumor region with higher accuracy, and the model is the combination of the W-Net and the BJA optimization. The model aids in achieving the absolute grades of the classification through enhanced segmentation.
- **BDN:** BDN represents the BHA-optimized DCNN that acts as the final classifier that classifies the segmented tumor acquired from the segmentation process. The model provides accurate classification with high efficiency.

The research article is structured as follows, Section 1 presents the research on BTs; Section 2 talks about current approaches to BT detection; Section 3 discusses the methods and their mathematical models; Section 4 examines the research model's outcomes; and Section 5 finalize the article with the future scope.

2. Literature review

The existing research articles on the detection of BT is analyzed and elaborated on along with the advantages and disadvantages in this section.

In [14], Marcin Wozniak *et al*., presented the Deep Neural Network (DNN) that worked with the correlation learning mechanism (CLM) to provide a robust classification. The utilization of the CLM enhances the learning ability of the model, which incorporates several filters to work with the noisy data. The model implemented in the research was the parallel processing model, which utilizes the multithread mechanism to follow up the research. The model ignored the advancements of the Convolutional neural network (CNN) such as the parallelization of pooling and the convolutional layer could be implemented to resolve the weights issue of the CNN. Amjad Rehman *et al*., [13] suggested the BT detection and classification model with an advanced 3D CNN model. The model provides a lower error rate and high accuracy in the classification of the tumor. Furthermore, the CbFNN mechanism in the selection of the appropriate features provided accurate results in the segmentation as well as the selection of the segmented features. However, the model required computational time, and the classification model utilized in the research needed to be replaced with the deep reinforcement models to achieve better efficacy in the BT detection.

Chirodip Lodh Choudary *et al*., [20] demonstrated the Deep CNN (DCNN) in the detection of the BT. The model utilized only the DCNN to perform the feature extraction as well as the classification or detection of the BT. The model needed to include the neutrosophical principles in the detection, which required the advanced mechanisms in preprocessing, and feature extraction, Moreover, the model could improve working with the classification models that include the bio-inspired algorithms or the advanced learning algorithms. In [3], Md Khairul Islam *et al*., included a template-based K-means clustering algorithm that detected the BT. The model included the superpixels and the PCA, which aided in achieving better feature extraction with the reduced dimensions. The major challenge concerned in the model was that the model worked with the small dataset, and could include the real-time dataset. The model could include using the advanced feature extraction mechanisms that should improve the classification accuracy, and in addition, the model could be included to work with the deep learning (DL) models to perform the seamless detection of the BT.

Mohammed Shahjahan Majib *et al*., [6] utilized the VGG-SCNet framework to detect BTs. The model used the stacked classifier, which was the combination of certain ML and DL algorithms that aid in extracting the accurate features of the tumor obtained from the MRI. The F1 score of the research is high, which reminds us that the method achieved relatable high performance. The unavailability of the benchmark dataset in the detection of BTs led to the poor performance of the DL models as they required larger data to process further. In addition, the model faced

difficulty in tuning the hyperparameters, and the trade-off between the utilized algorithms led to the complexity in time. In [21], Andres Anaya Isaza and Leonel Mera Jimenez modeled the framework that included the PCA to generate the images and in addition, the data augmentation was carried out with the Transfer learning mechanism. The major challenge of the model was the data augmentation mechanism that worked individually on each image, which could be incorporated to obtain the combined data from the single image resources. The model did not consider the noise rate of the generated data from the PCA, which led to the poor performance of the research in terms of detection accuracy.

D, Rammurthy, and P.K Mahesh in [5] elaborated the WHHO-based DeepCNN to outperform the existing researches. The segmentation of the research utilized the cellular automata and rough set theory that obtained the accurate segmentation with better preprocessing and feature extraction that enhanced the quality of the research through which better accuracy is achieved in the detection. The computation efficiency of the research was a bit low due to the incorporation of several efficient mechanisms. The advanced bio-inspired algorithms could be included to perform the extraction of the optimal weights of the classifier. In [22], Takowa Rahman and Md Saiful Islam introduced the parallel DCNN, where mechanisms such as data augmentation, data partitioning, and grayscale conversion were carried out in the research. The research obtained greater detection accuracy concerning the parallel processing of the data, which additionally, showed better feature enhancements.

2.1 Challenges

- A modified Softmax Loss Function and Regularization are required for CNN to improve the network's reliability and boost system efficacy. Moreover, DL models can be trained and tested using substantial datasets for various BTs [23].
- Even while 2D picture segmentation techniques can produce precise outcomes, some parametric data will be lost. Therefore, research on 3D brain medical imaging employing infrared detector imaging techniques and ML approaches is necessary [21].
- The Ensemble Learner Architecture handles various forms of larger datasets, but it lot of experimentation to achieve the necessary outstanding accuracy [5].
- The model needs to explore the minor tunings with large number of the techniques and the larger dataset that remains the challenge to classify BTs [24].

3. Detection and Classification of the Brain tumor with BW-Net+BDN

The research aims at developing a BT detection model specifically from the MRI images. To develop the optimal solution to the challenges of the conventional methods, the optimized Attentional CNN is developed that aims at detecting normal and abnormal tumors. The input of the research is obtained from two datasets namely, BT Segmentation (BraTS) 2017 [25] and BraTS 2020 [26] datasets, which contain the images as the outcome of the MRI. The input from the dataset is provided to the ROI Block that extracts the accurate tumor region from the entire image. The extracted ROI is utilized as the input to the BW-Net segmentation model that utilizes the W-Net, which is optimized with BJA optimization. The BW-Net segments the extracted images into the tumor and the non-tumor region, which aids in achieving better detection accuracy. Both the segmented images are provided in the feature extraction process, where the extraction of the statistical features, GLCM features, Grid-based features, and the pretrained VGG-16 feature takes place, which aids in achieving the enhanced detection of tumors. The BW-Net+BDN is employed as the classifier of the research, where the detection takes place, which is the incorporation of the Attentional mechanism and the BJA optimization into the basic CNN that achieves accurate detection of the normal and abnormal tumors. The utilized BJA optimization is the integration of the traits of the coyote and rabbit that tunes the hyperparameters of BW-Net+BDN. The Block diagram of the BT detection model is portrayed in Figure 1.

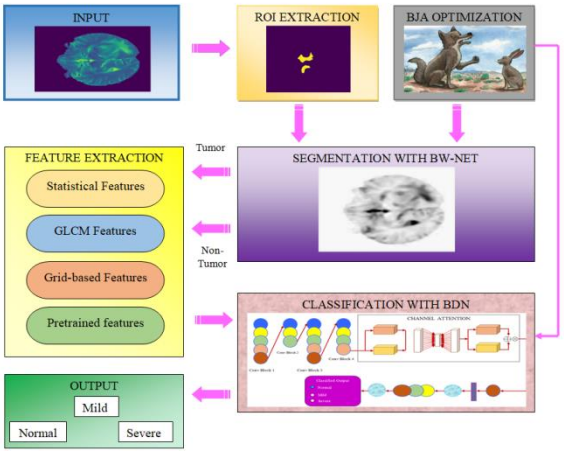

Fig. 1: Block Diagram of the BW-Net+BDN in BT Detection.

3.1 Input Image

BraTS 2017 and BraTS 2020 are employed as the input in the research of BT detection. The BraTS contains the MRI images without the labeling, which is eligible for all the brain disease tasks. The input obtained from the dataset is represented as,

$$I = \left\{ I_1, I_2, ..., I_i, ..., I_s \right\}, \quad (1)$$

where, s, is the total data available in the dataset I.

3.2 ROI Extraction with Adaptive Thresholding

ROI extraction extracts the point of interest that enhances the region of the tumor from the background artifacts. The adaptive thresholding mechanism is utilized to perform the ROI extraction [27]. Initially, the interesting point is extracted to classify the region of tumor or non-tumor, which is based on the threshold. The interested and not-interested pixels are represented as follows,

$$\left.\begin{aligned} I_i \in N_t, \quad & if\ I_i > Threshold\,T \\ I_i \in AN_t, \quad & if\ I_i \le Threshold\,T \end{aligned}\right\}, \tag{2}$$

The threshold that aids in determining the interested pixel is adaptive as the processor shifts between the local and the global thresholds, where local thresholds determine the unfixed intensity varying thresholds, whereas the global thresholds are the fixed background pixels. The estimation of the threshold with the varying pixels is represented as,

$$Threshold\,T = \left[\max\left(I_i\right) + \min\left(I_i\right)\right] / 2, \tag{3}$$

The ROI Extracted images are collectively represented as, r.

3.3 Segmentation of the ROI extracted Image with BW-Net

Segmentation segments the tumor and the non-tumor regions from the ROI-extracted Image. The W-Net is specifically employed in the research to provide précised outcomes, and the W-Net is optimized with certain optimization to ensure the tuned hyperparameters of the W-Net without the labeling information [28].

A single autoencoder is created by joining two fully convolutional network U-Net models together to form W-net, a completely unconstrained image segmentation model. While the other network functions as a decoder and produces a recreated image, the first fully convolutional network acts as an encoder and produces a segmented output. By establishing a relationship between the input and the output, the encoder-decoder models can learn. The design consists of two parts: the Encoder, which extracts the feature map and uses a network to process individual pixels to improve estimation, is the first part. The architecture's second component, the decoder, will retrieve the features that the encoder was able to collect with excellent resolution. While the decoder processes the recreated image, the encoder layer generates a segmented output. The optimization of the encoder will involve lowering the Soft N-cut loss, whereas the optimization of the decoder will involve decreasing the reconstruction loss [29].

The 14 modules represented in Figure make up the W-Net architecture's 28 convolutional layers. Two 3×3 convolutional layers make up each module. Each is followed by batch normalization (BN) [30], ReLU [31], and non-linearity. The network's deep forecast base is made up of the first seven modules, while the reconstruction decoder is represented by the last seven. Like with the original U-Net architecture, the En is composed of an expanding path that allows for exact localization and a contracting path to record context. The first module in the contracting path processes incoming images by convolution. Each down-sampling step doubles the amount of feature channels, and modules are coupled by 2×2 max-pooling layers. Modules in the expanding path are linked through 2D convolution layers that have been reversed. At every stage of upsampling, we reduce the total amount of feature channels by half. To recover lost spatial information from downsampling, each module's input in the contracted path is likewise bypassed and sent to its equivalent module's output in the expansive path. The final convolutional layer the En is a 1×1 convolution, which is followed by a softmax layer. Each 64-component feature vector is first mapped by the 1×1 convolution to the required number of classes. The Dec, architecture is comparable to that of the En, with the exception that it reads the En 's output. [28].

A. Soft Normalized Cut Loss

One method that is said to be graph-based is normalized cut loss when taking a set of vertices and placing them in a space to create the graph. The graph contains a node, which is a point and an edge is made up of two points. The similarity of the two sets, when the graph is divided can be estimated by eliminating the weights of the edge connecting the two sets. This process is termed as cut and the cut value should be minimized through the ideal partition. Normalized Cut Loss (N-cut loss) is estimated as the ratio of the number of nodes to the number of edges available in the partitions [32]. Several strategies have been developed to achieve the number of clusters proportionate to the image content. Due to the maximized N-cut loss, the correlation of the partitions will be maximized. To minimize the soft N-cut loss as well as the reconstruction loss, BW-Net is trained to perform the segmentation, and the outcome of the soft N-cut loss is represented as, W_{soft}.

B. Reconstruction Loss

Researchers train the BW-Net to reduce the reconstruction loss, just like in the conventional encoder-decoder architecture, to ensure that the encoded depictions retain as much data as possible from the initial inputs. The alignment of the segmentation estimate with the input images reduces the reconstruction loss. The amount lost to reconstruction is provided by.

$$W_{reconst} = \left\| r - Dec\left(En\left(r; W_{En}\right) W_{Dec}\right)\right\|_2^2, \quad (4)$$

where, N_t is the input image, W_{En}, and W_{Dec}, stand for the encoder and decoder parameters respectively. To decrease the $W_{reconst}$, between the original inputs and the reconstructed images, the W-Net is trained accurately. To optimize the linkage within segments and reduce disconnect between segments in the encoding layer, we simultaneously train En, to minimize W_{soft}. The network strikes a balance between the accuracy of the reconstruction and the consistency of the encoded representation layer by repeatedly applying $W_{reconst}$, and W_{soft}. The final segmented tumor region T_o and nontumor region T_I are collectively represented as, H.

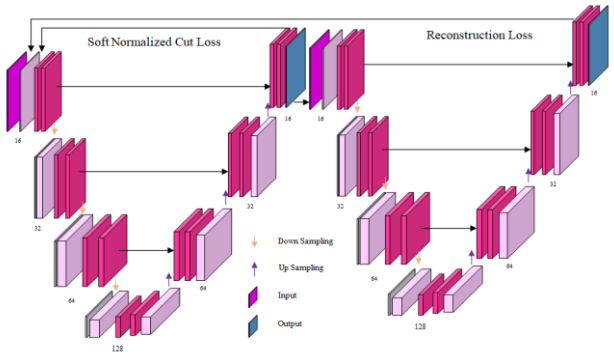

Fig. 2: BW-Net in Segmentation of the RoI images.

3.4 Feature extraction of the segmented Images

Feature extraction is to extract the most significant features of segmented image to perform the classification of the tumor into several grades or stages of tumor growth. The feature extraction process is performed using the pixel statistic measures, GLCM features, grid-based Features, and the pre-trained VGG-16 features.

3.4.1 Pixel Statistics Measures

Mean, Standard deviation, Variance, Skewness, Kurtosis, Maximum, and Minimum of the pixel intensities of the segmented tumor and the nontumor images are employed for the extraction of the features. The utilized pixel statistic measures in the research of BTs capture the visual content of the image that is used in the indexing and retrieval process [33]. The advantageous characteristics exhibited from the extraction of the pixel statistic measures aid in reducing the issue of overfitting, which in turn maximizes the accuracy obtained in the classification of the tumor grades. Furthermore, the extraction provides improved data visualization and thus, fastens the mode of training the model. The statistical features of the segmented tumor and non-tumor images T_j are mathematically described in Table 1,

Table 1: Mathematical description of Pixel statistic Measures.

Statistical Features	Formula
Mean M	$M = \frac{1}{2}\sum H$
Variance V	$V = \frac{1}{2}\sum\left(H - M\right)^2$
Kurtosis K	$K = \frac{1}{2}\sum\left(H_{j\in(0,1)} - M\right)^4$
Skewness S	$S = \frac{1}{2}\sum\left(H - M\right)^3$
Minimum Min	$Max = Max\left(H\right)$
Maximum Max	$Min = Min\left(H\right)$
Standard Deviation σ	$\sigma = \sqrt{\frac{1}{2}\sum\left(H - M\right)^2}$

The described pixel statistic measures are combined as, $STF = \left[M \,||\, V \,||\, S \,||\, K \,||\, Max \,||\, Min\right]$.

3.4.2 GLCM Features

The GLCM features utilized to perform the feature extraction are Dissimilarity, Homogeneity, Correlation, Contrast, Energy, and Entropy. The contrast in the image describes the local grey level variation and the texture, and edge obtained with the high contrast values, whereas the homogeneity of the segmented image describes the smoothness of the segmented image. The energy in the image expresses the uniformity by obtaining the square of the elements with the GLCM images [33]. Furthermore, the Entropy is estimated as the disorders in the obtained matrices of the image, which is inversely proportional to the energy. The utilized features provide better extraction of features that aid in achieving the maximum efficiency of grading the segmented tumor and non-tumor images. The estimated GLCM features are concatenated and represented as, $GLCM$, with the dimension of $\left(1\times 6\right)$.

3.4.3 Grid-based Features

Grid-based feature extraction involves dividing an image into a grid or a set of smaller regions called cells. Each grid cell represents a local region of the image. Features are then extracted from each cell independently. Initially, the image is divided into a grid of cells, which can be uniform or adaptive. Extraction of the grid cell features is performed with the appropriate feature extraction methods

such as the Mean, Variance, Skewness, and Kurtosis. The extracted features from all cells are combined to form a feature vector for the complete image, and the utilization of the grid-based feature extraction is due to certain advantages such as localization, robustness, and the scalability of the obtained features. The obtained features of the grid-based feature extraction is termed as, G, of (1×37)

3.4.4 Extraction of features with Pretrained VGG-16

One of the important CNN modulations to come out of the VGG-Net category is VGG-16. The main advantage of using VGG-16 is that its pretrained version can operate with millions of images [34]. The VGG-16 is different from the earlier iterations of the CNN modifications in terms of how it uses several compressively stacked filters. VGG-16 serves as the feature extractor in the BT classification research since it applies the same number of filters to the working layer several times, improving feature extraction. The outcome of the features from VGG-16 is obtained before the FCL block. The architecture includes 5 convolutional blocks with 13 convolutional layers followed by the implementation of the max pooling. The feature vector obtained from VGG-16 is in the dimension of $[1\times100]$ and is represented as, Vgg, which is depicted in Figure 3.

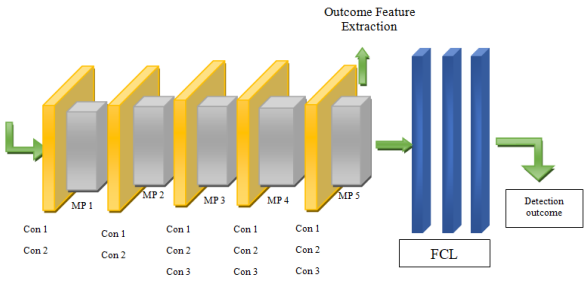

Fig. 3: VGG-16- Feature extractor

The obtained features in the feature extraction are considered for both tumor and nontumor regions of the segmented image and the concatenated outcome is represented as, $F_{vec}(T_o)$, and $F_{vec}(T_1)$ for both tumor and the non-tumor regions respectively.

3.5 Classification of the BT with the BDN

The classification of grades of the BT is performed with BDN, which includes the Deep CNN, which is optimized with the BHA optimization. The fundamental DL architecture, DCNN, is made up of three primary levels: convolutional, pooling, and fully connected (FCL). A convolutional layer processes short localized portions of the feature map that is extracted of the initial input by applying a set of weights known as a kernel. Clusters of neurons make up feature maps and by the use of the filter bank, every feature map of the current convolutional layer is linked to the neighborhood boundaries preceding the layer. After that, a non-linear function like a Sigmoid, Tanh, or Rectified Leaky Unit (ReLU) is applied to the total of the localized weights [35]. Notably, distinct feature maps in a convolutional layer employ distinct filters, whereas all units within a single feature map utilize the same filter. While the pooling layer combines related features into a single one, the convolutional layer aids in the discovery of specific links between features from the preceding layer. Adjacent units exhibit correlation with one another producing a feature map with a lower resolution can facilitate reliable detection. In addition to creating invariance to translation and distortion, the pooling layer can reduce the number of parameters and the dimension of feature maps. Typically, there are a few FCLs after the DCNNs [36]. The final class vector is produced by Top FCL after classifying the tumor task's grades. The proposed research incorporated the attention mechanism along with the DCNN, which is depicted in Figure 4.

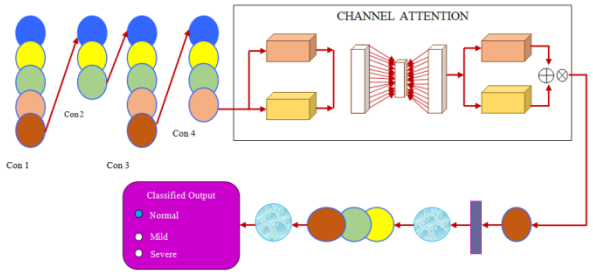

Fig. 4: Workflow of the BDN in BT detection.

3.5.1 Channel Attention Mechanism

The channel attention module utilized in the research is the basic technique to inclchannel-wise information through the relation of the MRI data [37]. For input, two descriptors such as the max-pooling and average-pooling of particular data can be calculated in the following,

$$Max_{pool} = Max\left(F_{vec}(h,w,d)\right), \tag{5}$$

$$Avg_{pool} = \frac{1}{h\times w\times d}\sum F_{vec}(h,w,d), \tag{6}$$

where, h,w,d, represents the height, width, and depth of the particular channels where the max pooling and the average pooling are executed. The descriptors are transmitted into the single convolutional layer and the Channel-wise addition and Sigmoid activation are estimated as the weighted outcome of each channel that obtains the channel attention map C.

$$C = \sigma\left(Con\left(Max_{pool}\right)+Con\left(Avg_{pool}\right)\right), \tag{7}$$

3.5.2 Brilliant Jumping Algorithm Optimization

BJA optimization is the integration of the detour foraging traits of the rabbit [38], and the intelligence characteristics of the Coyote [39] are the traits for searching the food. The optimization achieves accurate classification of the BT based on the grades of the tumor.

Inspiration: Hares belong to the Leporid family and are sometimes referred to as rabbits. The BJA algorithm considers that to protect themselves from attackers and trappers, hares dig trenches around their nests and employ a haphazard hiding technique. The inspiration comes from these innate survival techniques. These creatures stay away from their nests to prevent being found by predators, and they primarily eat grass and green plants. Canis Latrans, the species of coyote, is a mammal found in North America. The algorithm is designed to account for the way coyotes arrange their social relationships and adapt to their environment, with a focus on how they pool their resources and cooperate to attack their prey.

Initialization: The solution of the optimization is declared as, E, at the particular iteration q, which is based on the initialization of the population on the search space.

$$E^q = lwr + upr\left(E_{\max} - E_{\min}\right), \tag{8}$$

where, lwr, represents the lower boundary, and upr, is the upper boundary.

Loss function: The loss function of the classifier is majorly concerned with the maximum accuracy, which is denoted as, R.

$$R\left(E^q\right) = Max\left(Accuracy\left(E^q\right)\right), \tag{9}$$

Solution Update: The solutions of the phases are arranged and updated on each phase and the conditions are chosen based on the probability of the distance between the food and solution, a random function.

Phase 1: $D_p > \gamma$ Lead and Attack Phase**:** In the leading phase, when there is no predator, the prey searches for the food source, utilizing the deviated grazing technique. In search of the best solution, the deviated grazing technique is replaced with the fittest solution.

$$E^{q+1} = 0.5\left[E^q + \alpha\left(E_{per} - E^q\right) + e_1\delta_1 + e_2\delta_2\right] + 0.5\left[E^q + F\left(E^q - E_{mean}\right) + 0.5\left(0.05 + e_3\right).n + v^{q+1}\right], \tag{10}$$

where, E_{per}, is the personal solution, α, is the cooperative hunting factor that ranges (0,1), e_1, e_2, and e_3, is the sound factor coefficients, F, is the stochastic factor, n, represents the population that belongs to the total population L, v^{q+1}, is the velocity at the next iteration $q+1$.

Phase 2: $D_p \le \gamma$ Lead and Escape Phase: The prey is in danger as the predator is found in the search space, then the entire pack hides in the nest using the unique communicative behavior, and the specific jump mechanism followed by the prey. Thus, the escape mechanism is executed successfully. The updated solution is as follows,

$$E^{q+1} = 0.5\left[E^q + \alpha\left(E_{per} - E^q\right) + e_1\delta_1 + e_2\delta_2\right] + 0.5\left[E^q + F\left(e_4\left(E^q + l.m.E^q\right)\right) - E^q\right], \tag{11}$$

where, l, is the iterative factor, m, is the mutative factor, and e_4, is the exponential factor, which is represented as,

$$e_4 = \left|\frac{q_{\max} - 1}{q_{\max} + 1}\right|, \tag{12}$$

The best solutions are updated based on the updated phase.

Reevaluate the Loss function: The loss function of the re-evaluated is held as per the updated solutions.

Termination Condition: When $q > q_{\max}$, iteration ends, and the best solution is declared. The phases are depicted in Figure 5.

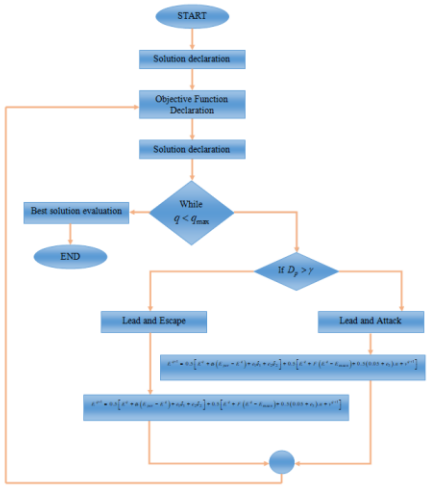

Fig. 5: BHA optimization-Flowchart.

4. Results

The outcomes in the research of BT detection are analyzed in this section.

4.1 Experimental Setup

The experiment is performed in the system with Windows 10 configuration and 16 GB RAM storage. The implementation of the code is carried out in Python software.

4.2 Dataset description

BraTS 2017 and BraTS 2020 are the datasets employed in the research of BT classification. The Datasets include MRI images of 210 high-grade gliomas and 75 low-grade gliomas that form the training set and 46 cases to form the validation set [40]. The data of the dataset can be utilized in several areas of interest such as segmentation of tumors, data clarification of the survival, and progression, and so on.

4.3 Experimental Outcomes

The experimental results of each stage of BT detection are illustrated in Figure 6.

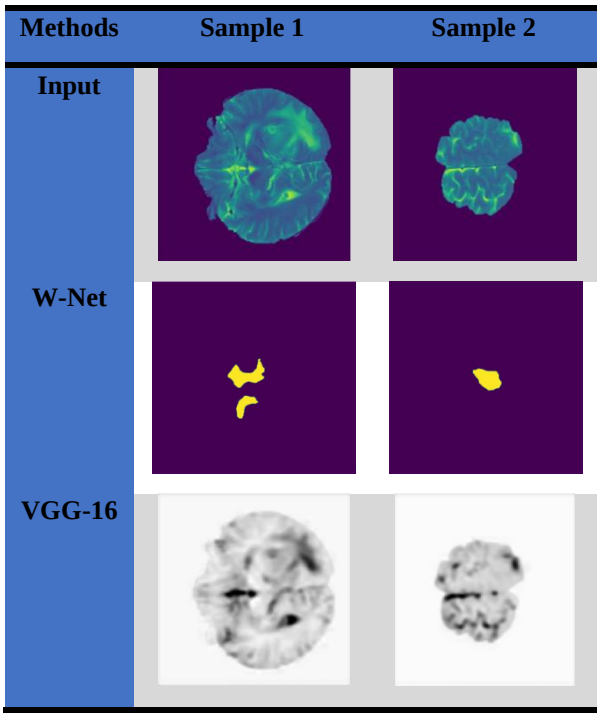

Fig. 6: Experimental Results of the BW-Net+BDN model in the detection of BT.

4.4 Performance Metrics

The performance metrics involved in the research are Accuracy, Sensitivity, Specificity, and the Balanced Error Rate. The accuracy is the measure that shows the correctly identified tumors and the non-tumors, thus providing a straightforward understanding of the performance of the model. While the sensitivity of the BT detection represents the predicted positive cases to the available positive tumor cases, the specificity represents the predicted negative cases, which aids in achieving the prior information of the consequences of both the positive and the negative cases. The balanced error rate is the combination of the sensitivity and the specificity, in overall the average of the errors obtained in each class. This balanced error rate balances the trade-off issue between sensitivity and specificity and estimates the accurate positive and negative cases through a model of BT detection. In the proposed research on BT detection, the metrics show higher performance.

4.5 Performance Analysis

The performance analysis of the datasets BraTS 2017 and BraTS 2020 are performed in this section, where the epoch 500 remains constant concerning the varying training percentage (TP) that shows the improved performance of the BW-Net+BDN model in the research of BT detection.

4.5.1 BraTS-2017 Dataset

The accuracy of the BW-Net+BDN model shows 86.68%, 90.45%, 91.66%, 91.89%, 92.28%, and 93.18% with TP 40, 50, 60, 70, 80, and 90 respectively. The sensitivity of the model provides 84.40%, 91.44%, 91.55%, 91.89%, 91.92%, and 93.34% with the respective TPs. The specificity of the BW-Net+BDN model presented 88.97%, 89.47%, 91.77%, 91.89%, 92.65%, and 93.02% with the respective TPs, whereas the balanced error rate with the respective TPs are 13.17, 9.97, 8.72, 8.47, 7.74, and 7.30. The entire performance of the BraTS 2017 is given in Figure 7.

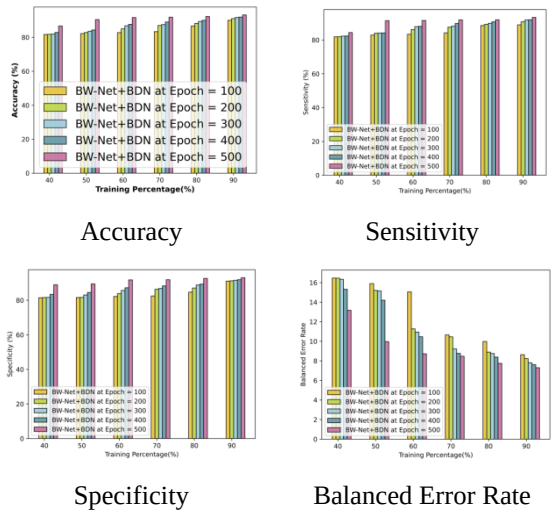

Fig. 7: Performance Analysis of BraTS 2017.

4.5.2 BraTS-2020 Dataset

The accuracy of the BW-Net+BDN model shows 88.46%, 90.90%, 91.10%, 92.21%, 92.70%, and 93.58% with TP 40, 50, 60, 70, 80, and 90 respectively. The sensitivity of the model provides 89.06%, 91.02%, 91.02%, 92.74%, 92.79%, and 93.39% with the respective TPs. The specificity of the BW-Net+BDN model presented 87.86%, 90.77%, 91.17%, 91.67%, 92.61%, and 93.77% with the respective TPs, whereas the balanced error rate with respective TPs are 10.55, 7.83, 7.63, 7.41, 6.83, and 6.58. The entire performance of the BraTS 2020 is shown in Figure 8.

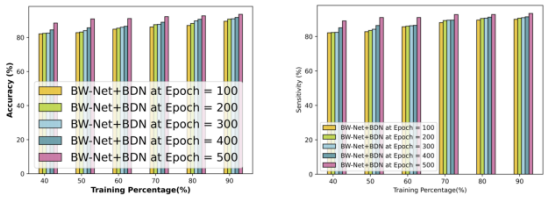

Accuracy Sensitivity

Specificity Balanced Error Rate

Fig. 8: Performance Analysis of BraTS 2020.

4.6 Comparative Analysis

The comparative analysis of the research depicts the comparison of the proposed BW-Net+BDN model in the detection of BTs with the existing research models such as Naïve Bayes (NB) [41], Multilayer Perceptron (MLP) [42], CNN-Long Short Term Memory (CNN-LSTM) [43], DCNN [23], Artificial Rabbit optimization based DCNN (ARDN) [38], Coyote Optimization Algorithm based DCNN (CODN) [39].

4.6.1 BraTS 2017 dataset Analysis

The comparison in terms of accuracy with the existing methods shows an improvement of 9.64% with NB, 10.30% with MLP, 11.93% with CNN-LSTM, 0.90% with DCNN, 4.74% with ARDN, and 2.37% with CODN. The sensitivity shows the enhancement of 7.09%, 12.34%, 14.33%, 0.22%, 2.07%, and 1.82% with the respective conventional methods. The specificity of the research provides the improvement of 12.21%, 8.25%, 9.51%, 1.59%, 7.42%, and 2.92% with NB, MLP, CNN-LSTM, DCNN, ARDN, and CODN respectively. The balanced Error rate with the improvement of 12.77, 13.54, 10.27, 4.97, 1.72, and 2.21 with NB, MLP, CNN-LSTM, DCNN, ARDN, and CODN respectively are shown in the research. The illustration is illustrated in Figure 9.

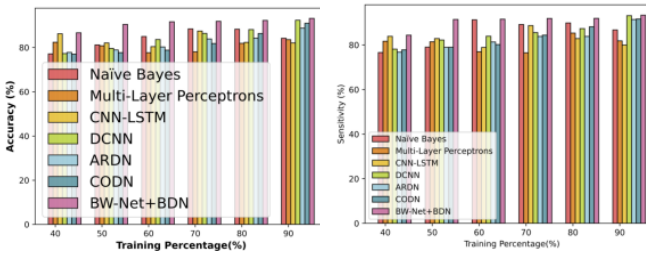

Accuracy Sensitivity

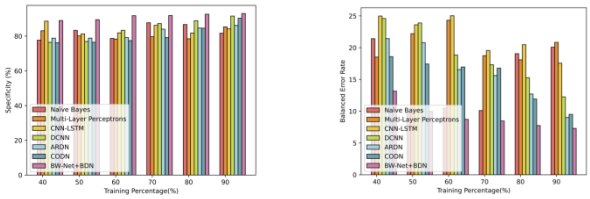

Specificity Balanced Error Rate

Fig. 9: Comparative Analysis of BraTS 2017.

4.6.2 BraTS 2020 Dataset Analysis

The comparison in terms of accuracy shows an improvement of 13.21% with NB, 13.16% with MLP, 12.30% with CNN-LSTM, 5.03% with DCNN, 7.19% with ARDN, and 5.80% with CODN. The sensitivity shows the enhancement of 12.33%, 14.85%, 12.43%, 4.12%, 10.06%, and 4.35% with the respective conventional methods. The specificity of the research provides the improvement of 14.08%, 11.47%, 12.17%, 5.94%, 4.34%, and 7.24% with NB, MLP, CNN-LSTM, DCNN, ARDN, and CODN respectively. The balanced Error rate with the improvement of 14.37, 14.33, 9.20, 5.99, 4.17, and 1.63 with NB, MLP, CNN-LSTM, DCNN, ARDN, and CODN respectively are shown in the research. The illustration is depicted in Figure 10.

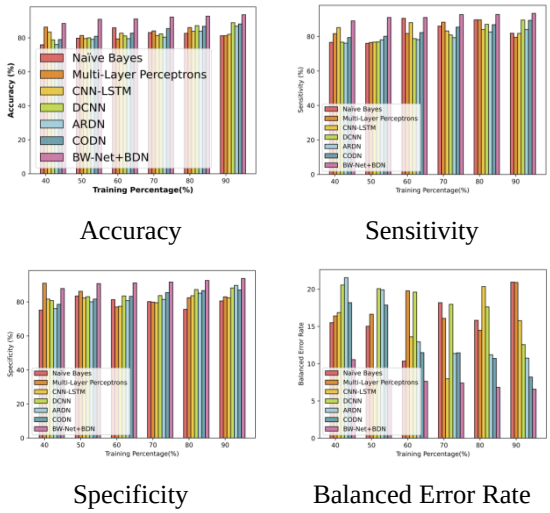

Accuracy Sensitivity

Specificity Balanced Error Rate

Fig. 10: Comparative Analysis of BraTS 2020.

4.7 Comparative Discussion

The conventional and the proposed BW-Net+BDN are compared based on the performance and the comparison is tabulated in Table 2. CNN-LSTMs excel at classifying images that closely resemble the training dataset. However, when faced with images containing scaling, CNN-LSTMs struggle to classify them accurately. BT images with varying angles or tilts pose a challenge for CNN-LSTMs. Data augmentation during training can mitigate this issue, but it remains a limitation. DCNNs are computationally expensive due to their deep architecture.

Training and inference times can be lengthy, especially when dealing with large medical image datasets. Real-time applications may suffer from latency. MLPs lack the ability to capture spatial information effectively. In BT detection, spatial relationships between pixels are crucial for accurate diagnosis. MLPs treat input data as flat vectors, ignoring the inherent structure of images. NB assumes independence between features, which is often unrealistic for complex medical data. BT images exhibit intricate correlations between pixels, making the independence assumption inappropriate. To overcome the drawbacks of the comparative methods, the BW-Net+BDN is proposed in the research that achieves high accuracy.

Table 2: Comparative Discussion of BT Detection.

Analysis/Methods			**NB**	**MLP**	**CNN-LSTM**	**DCNN**	**ARDN**	**CODN**	**BW-Net+BDN**
TP	**BraTS 2017**	**Accuracy (%)**	84.20	83.59	82.07	92.34	88.76	90.97	93.18
		Sensitivity (%)	86.73	81.83	79.97	93.14	91.41	91.64	93.34
		Specificity (%)	81.67	85.35	84.17	91.54	86.12	90.30	93.02
		Balanced Error Rate	20.07	20.84	17.57	12.26	9.02	9.51	7.30
	BraTS 2020	**Accuracy (%)**	81.22	81.27	82.07	88.87	86.85	88.16	93.58
		Sensitivity (%)	81.88	79.53	81.78	89.55	84.00	89.33	93.39
		Specificity (%)	80.57	83.02	82.36	88.20	89.71	86.99	93.77
		Balanced Error Rate	20.95	20.91	15.78	12.56	10.75	8.21	6.58

5. Conclusion

The BW-Net+BDN is employed in the research of detecting and classifying the BTs with high proficiency. The research included W-Net as the segmentation model that is optimized with the Brilliant jumping Algorithm (BJA). Furthermore, the included optimization is the hybridization of the characteristics of the rabbit as well as the coyote to enhance the efficiency of the classifier and the segmentation model as optimization is utilized in both classification and segmentation. The entire research detects the BT through the BW-Net segmentation model and classifies them based on grades such as normal, mild, and severe through the BDN classification model. The performance of the research is analyzed with accuracy, Sensitivity, Specificity, and Balanced Error Rate that achieves 93.23%, 93.39%, 93.77%, and 6.58 respectively. In the future, the research can be improved in terms of the classifier that can be included with the recent learning algorithms to provide the high-efficiency outcomes.

References

[1] M.S. Alam, M.M. Rahman, M.A. Hossain, M.K. Islam, K.M. Ahmed, K.T. Ahmed, B.C. Singh, and M.S. Miah,"Automatic human brain tumor detection in MRI image using template-based K means and improved fuzzy C means clustering algorithm." Big Data and Cognitive Computing, 2019, 3(2), p.27.

[2] M.K. Islam, M.S. Ali, A.A. Das, D. Duranta, and M. Alam, "Human brain tumor detection using k-means segmentation and improved support vector machine." International Journal of Scientific Engineering Research, 2020, 11(6), p.6.

[3] M.K. Islam, M.S. Ali, M.S. Miah, M.M. Rahman, M.S. Alam, and M.A. Hossain, "Brain tumor detection in MR image using superpixels, principal component analysis and template based K-means clustering algorithm." Machine Learning with Applications, 2021, 5, p.100044.

[4] Brain Tumor. Accessed: Apr. 11, 2021. [Online]. Available: https://www. healthline.com/health/brain-tumor

[5] D. Rammurthy, and P.K. Mahesh, "Whale Harris hawks optimization based deep learning classifier for brain tumor detection using MRI images." Journal of King Saud University-Computer and Information Sciences, 2022, 34(6), pp.3259-3272.

[6] M.S. Majib, M.M. Rahman, T.S. Sazzad, N.I. Khan, and S.K. Dey, "Vgg-scnet: A vgg net-based deep learning framework for brain tumor detection on mri images." IEEE Access, 2021, 9, pp.116942-116952.

[7] K. Ejaz, M.S.M. Rahim, A. Rehman, H. Chaudhry, T. Saba, A. Ejaz, and C.F. Ej, "Segmentation method for pathological brain tumor and accurate detection using MRI." International Journal of Advanced Computer Science and Applications, 2018, 9(8), pp.394-401.

[8] Rehman, M.A. Khan, Z. Mehmood, T. Saba, M. Sardaraz, and M. Rashid, "Microscopic melanoma detection and classification: A framework of

pixel-based fusion and multilevel features reduction." Microscopy research and technique, 2020, 83(4), pp.410-423.

[9] J. Amin, M. Sharif, M. Raza, T. Saba, R. Sial, and S.A. Shad, "Brain tumor detection: a long short-term memory (LSTM)-based learning model." Neural Computing and Applications, 2020, 32, pp.15965-15973.

[10] J. Amin, M. Sharif, M. Yasmin, T. Saba, and M. Raza, "Use of machine intelligence to conduct analysis of human brain data for detection of abnormalities in its cognitive functions." Multimedia Tools and Applications, 2020, 79, pp.10955-10973.

[11] F. Ramzan, M.U.G. Khan, S. Iqbal, T. Saba, and A. Rehman, Volumetric segmentation of brain regions from MRI scans using 3D convolutional neural networks. IEEE Access, 2020, 8, pp.103697-103709.

[12] M. Grade, J.A. Hernandez Tamames, F.B. Pizzini, E. Achten, X. Golay, and M. Smits, "A neuroradiologist's guide to arterial spin labeling MRI in clinical practice." Neuroradiology, 2015, 57, pp.1181-1202.

[13] Rehman, M.A. Khan, T. Saba, Z. Mehmood, U.Tariq, and N. Ayesha, "Microscopic brain tumor detection and classification using 3D CNN and feature selection architecture." Microscopy Research and Technique, 2021, 84(1), pp.133-149.

[14] M. Woźniak, J. Siłka, and M. Wieczorek, "Deep neural network correlation learning mechanism for CT brain tumor detection." Neural Computing and Applications, 2023, 35(20), pp.14611-14626.

[15] E.I. Zacharaki, S.Wang, S. Chawla, D. Soo Yoo, R. Wolf, E.R. Melhem, and C. Davatzikos, "Classification of brain tumor type and grade using MRI texture and shape in a machine learning scheme." Magnetic Resonance in Medicine: An Official Journal of the International Society for Magnetic Resonance in Medicine, 2009, 62(6), pp.1609-1618.

[16] E.S.A. El-Dahshan, T. Hosny, and A.B.M. Salem, "Hybrid intelligent techniques for MRI brain images classification." Digital signal processing, 2010, 20(2), pp.433-441.

[17] J. Cheng, W. Huang, S. Cao, R. Yang, W. Yang, Z. Yun, Z. Wang, and Q. Feng, "Enhanced performance of brain tumor classification via tumor region augmentation and partition." PloS one, 2015, 10(10), p.e0140381.

[18] E.I. Papageorgiou, P.P. Spyridonos, D.T. Glotsos, C.D. Stylios, P. Ravazoula, G.N. Nikiforidis, and P.P. Groumpos, Brain tumor characterization using the soft computing technique of fuzzy cognitive maps. Applied soft computing, 2008, 8(1), pp.820-828.

[19] P. Abdolmaleki, F. Mihara, K. Masuda, and L.D. Buadu, "Neural networks analysis of astrocytic gliomas from MRI appearances." Cancer letters, 1997, 118(1), pp.69-78.

[20] C.L. Choudhury, C. Mahanty, R. Kumar, and B.K. Mishra, "Brain tumor detection and classification using convolutional neural network and deep neural network." In 2020 international conference on computer science, engineering and applications (ICCSEA) 2020,pp. 1-4.

[21] Anaya-Isaza, and L. Mera-Jiménez, "Data augmentation and transfer learning for brain tumor detection in magnetic resonance imaging." IEEE Access, 2022, 10, pp.23217-23233.

[22] T. Rahman, and M.S. Islam, "MRI brain tumor detection and classification using parallel deep convolutional neural networks." Measurement: Sensors, 2023, 26, p.100694.

[23] H. Shrestha, C. Dhasarathan, M. Kumar, R. Nidhya, A. Shankar, and M. Kumar, "A deep learning based convolution neural network-DCNN approach to detect brain tumor." In Proceedings of Academia-Industry Consortium for Data Science: AICDS 2020 2022, 115-127.

[24] N. Noreen, S. Palaniappan, A. Qayyum, I. Ahmad, M. Imran, M. Shoaib, "A deep learning model based on concatenation approach for the diagnosis of brain tumor." IEEE Access. 2022, 55135-44.

[25] BraTS 2017 Dataset, https://www.med.upenn.edu/sbia/brats2017.html accessed on February, 2024.

[26] BraTS 2020 Dataset, https://www.med.upenn.edu/cbica/brats2020/ accessed on February, 2024.

[27] Y. Xia, L. Cheng, W. Li, and S. Ning, "A Region of Interest Extraction Approach Based on Adaptive Threshold in Intelligent Transportation System." In 2009 Asia-Pacific Conference on Information Processing, 2009, Vol. 2, pp. 120-123). IEEE.

[28] X.Xia, and B. Kulis, "W-net: A deep model for fully unsupervised image segmentation." arXiv preprint arXiv: 2017, 1711.08506.

[29] E.S. Saleh, T.M. Haridas, and M.H. Supriya, "Unsupervised image segmentation model based on w net architecture and conditional random field for underwater images." In 2021 7th International

Conference on Advanced Computing and Communication Systems (ICACCS) 2021, Vol. 1, pp. 34-39.

[30] S. Ioffe, and C. Szegedy, "Batch normalization: Accelerating deep network training by reducing internal covariate shift." In International conference on machine learning, 2015, pp. 448-456). pmlr.

[31] V. Nair, and G.E. Hinton, "Rectified linear units improve restricted boltzmann machines." In Proceedings of the 27th international conference on machine learning (ICML-10) 2010., pp. 807-814.

[32] J. Shi, and J. Malik, "Normalized cuts and image segmentation." IEEE Transactions on pattern analysis and machine intelligence, 2000, 22(8), pp.888-905.

[33] S.M. Vijithananda, M.L. Jayatilake, B. Hewavithana, T. Gonçalves, L.M. Rato, B.S. Weerakoon, T.D. Kalupahana, A.D. Silva, and K.D. Dissanayake, Feature extraction from MRI ADC images for brain tumor classification using machine learning techniques. Biomedical engineering online, 2022, 21(1), p.52.

[34] S. Tammina, "Transfer learning using vgg-16 with deep convolutional neural network for classifying images." International Journal of Scientific and Research Publications (IJSRP), 2019, 9(10), pp.143-150.

[35] S. Kumar, R. Dhir, and N. Chaurasia, "Brain Tumor Detection Analysis Using CNN: A Review." In 2021 International Conference on Artificial Intelligence and Smart Systems (ICAIS) 2021, 1061-1067.

[36] J. Amin, M. Sharif, N. Gul, M. Yasmin, and S.A. Shad, "Brain tumor classification based on DWT fusion of MRI sequences using convolutional neural network." Pattern Recognition Letters, 2020, 129, pp.115-122.

[37] Y. Yao, P. Qian, Z. Zhao, and Z. Zeng, "Residual Channel Attention Network for Brain Glioma Segmentation." In 2022 44th Annual International Conference of the IEEE Engineering in Medicine & Biology Society (EMBC) 2022, pp. 2132-2135.

[38] A.E. Khalil, T.A. Boghdady, M.H. Alham, and D.K. Ibrahim, "Enhancing the conventional controllers for load frequency control of isolated microgrids using proposed multi-objective formulation via artificial rabbits optimization algorithm." IEEE Access, 2023, 11, pp.3472-3493.

[39] Z. Yuan, W. Wang, H. Wang, and A. Yildizbasi, "Developed coyote optimization algorithm and its application to optimal parameters estimation of PEMFC model." Energy Reports, 2020, 6, pp.1106-1117.

[40] C. Zhou, C. Ding, X. Wang, Z. Lu, and D. Tao, "One-pass multi-task networks with cross-task guided attention for brain tumor segmentation." IEEE Transactions on Image Processing, 2020, 29, pp.4516-4529.

[41] G. Kaur, and A. Oberoi, "Novel approach for brain tumor detection based on Naïve Bayes classification." In Data Management, Analytics and Innovation: Proceedings of ICDMAI 2019, 1, pp. 451-462.

[42] Y. Ayyappa, A. Bekkanti, A. Krishna, P. Neelakanteswara, and C.Z. Basha, "Enhanced and effective computerized multi layered perceptron based back propagation brain tumor detection with Gaussian filtering." In 2020 Second International Conference on Inventive Research in Computing Applications (ICIRCA), 2020, pp. 58-62.

[43] S. Montaha, S. Azam, A.R.H. Rafid, M.Z. Hasan, A. Karim, and A. Islam, "Timedistributed-cnn-lstm: A hybrid approach combining cnn and lstm to classify brain tumor on 3d mri scans performing ablation study." IEEE Access, 2022, 10, pp.60039-60059.